Electronic Supplementary Material (ESI) for Nanoscale.

Supplementary Information for:

Dynamic reconfiguration of van der Waals gaps within GeTe-Sb_2Te_3 based superlattices

Jamo Momand[1,*], *Ruining Wang*[2], *Jos E. Boschker*[2], *Marcel A. Verheijen*[3], *Raffaella Calarco*[2], *Bart J. Kooi*[1,*]

[1]Zernike Institute for Advanced Materials, University of Groningen, Nijenborgh 4, 9747 AG Groningen, The Netherlands

[2]Paul-Drude-Institut für Festkörperelektronik, Hausvogteiplatz 5-7, 10117 Berlin, Germany

[3]Eindhoven University of Technology, Department of Applied Physics, 5600 MB Eindhoven, The Netherlands

*E-mail: j.momand@rug.nl, b.j.kooi@rug.nl

1. Interpretation of HAADF intensities in GeSbTe

The metastable and stable crystalline phases of GeSbTe (GST) have been widely studied using different experimental techniques including X-Ray Diffraction (XRD)[1–6] and (Scanning) Transmission Electron Microscopy ((S)TEM).[7–12] Reviewing these references one can conclude the following:

- Metastable GST has a distorted rocksalt structure where the anion lattice is fully (= 1) occupied by Te and the cation lattice is randomly occupied by Ge/Sb/vacancies.
- Stable GST is similar with the major differences that van der Waals (vdW) gaps have formed, containing adjacent Te-Te atomic planes in its stacking, and the distribution of Ge/Sb is such that the Sb-richer planes are closer to vdW gaps and Ge richer planes are at the centers of the blocks.
- Anti-site disorder is not significant in the stable phase of GST.
- The HAADF intensity scales approximately between $Z^{1.7}$ and Z^{2}.

Using these structural properties HAADF-STEM micrographs of GST phases can qualitatively be interpreted without ambiguity, as for example shown in Figure S1 below.

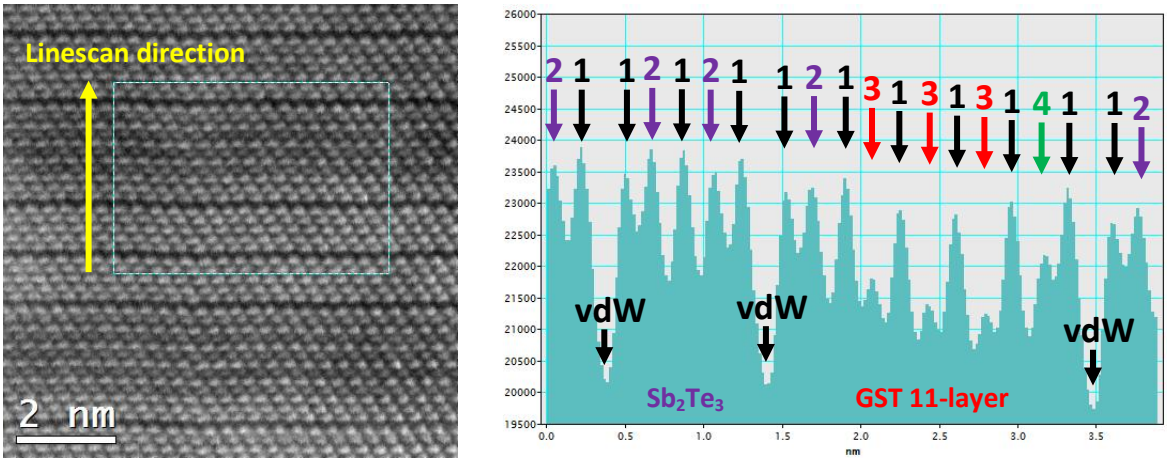

Figure S1: Interpretation of HAADF-STEM micrographs (left) using intensity linescans (right).

1. The atomic planes next to the vdW gaps, as well as every alternate anion atomic plane in the growth direction, must be close to pure Te planes (see black arrows). Note that the intensity is not fully homogeneous across the image. This is a specimen preparation artifact which can be due to specimen thickness variation and/or amorphous damage variation.

2. Adjacent to the Te must be Ge/Sb planes. Since the HAADF intensity scales with ~Z^2, where Z_{Ge} = 32, Z_{Sb} = 51 and Z_{Te} = 52, the other planes with intensities close to Te must be close to pure Sb (see purple arrows).
3. Due to deposition kinetics of SuperLattices (SL) the atomic planes with lowest intensities must be close to pure Ge (see red arrows).
4. The planes with intermediate intensities therefore must be mixed with Ge/Sb (see green arrow).

Looking across the linescan in Figure S1 (right) it becomes evident that the first vdW block is an Sb_2Te_3 quintuple layer (QL) and the second vdW block a GST 11-layer with a stacking sequence closely related to that proposed by Kooi *et al.* (Te-Sb-Te-Ge-Te-Ge-Te-Ge-Te-Sb-Te).[7] A more quantitative estimation of atomic species in GST using HAADF intensities should be done using simulations and can be found in other references in the literature.[8,10]

2. Mapping of vacancy layers and vdW gaps

To find the positions of vdW gaps the HAADF micrographs were frequently too noisy for peak-search algorithms, particularly for large overviews. Many images showed *e.g.* intensity gradients due to thinner and thicker regions of the specimen and/or amorphous damage. Geometric Phase Analysis[13] (GPA) on the other hand is less sensitive to such gradients as it makes use of the periodicity of the lattice with its deviation from the average. The resulting phase-maps distinguish inter-planar distances with high accuracy[14] and analysis could therefore be automated.

As this method is used for the analysis of multiple micrographs where the results should be compared, the input images are systematically rotated and calibrated to the same conditions. Then the GPA algorithm is applied and the phase-maps are processed by a simple peak-search script (as *e.g.* implemented in MATLAB software). The application of the GPA is done using the FRWR tools plugin in GMS, freely available at: https://www.physik.hu-berlin.de/en/sem/software/software_frwrtools. The detailed steps of this procedure are described below.

1. **STEM imaging:** For the acquisition of the images the "slow" STEM scanning direction was set approximately perpendicular to the substrate-film interface or vdW gaps to minimize image-distortions in the [0001] direction of the film, which were particularly prevalent for long scans due to drift and/or charging effects (Figure S2).

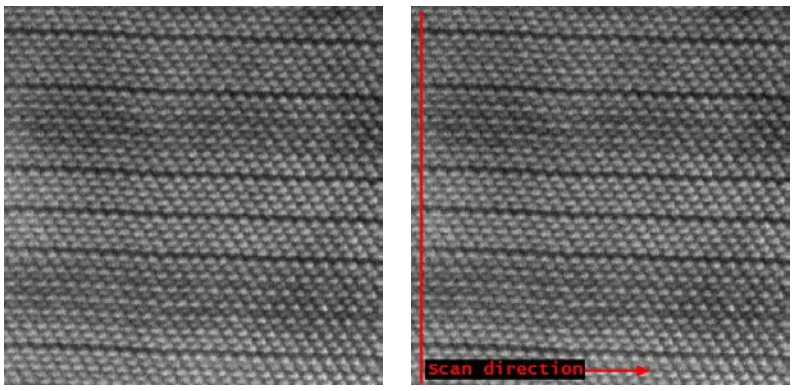

Figure S2: STEM scanning conditions and directions.

2. **Rotation and/or cropping of images**: The average [0001] direction of HAADF-STEM micrographs was found manually using FFT of the images. If this direction and the y-axis were off by more than 1°, the images were rotated and cropped to have the [0001] direction along the y-axis (Figure S3).

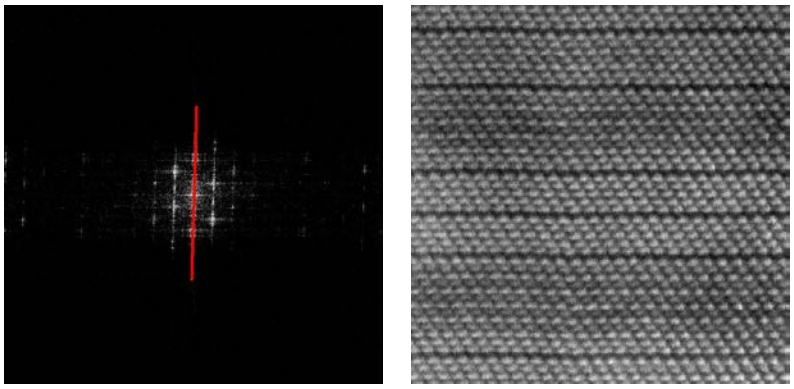

Figure S3: The [0001] direction is located in the FFT (left) and the image is rotated (right).

3. **Calibration**: All HAADF-STEM micrographs containing the Si substrate were analyzed. The (111) planes were measured along the [111] directions using either (*i*) polynomial fitting of the linescan peaks and/or (*ii*) the DIFPACK module of Gatan Inc.[15] Both methods (*i*) and (*ii*) gave the same results to within 1% difference. The calibration was set such that the Si(111) spacing was 0.3135 nm.[16] For images not containing the substrate, the calibration was set applying the previously found calibration number with the magnification (Figure S4).

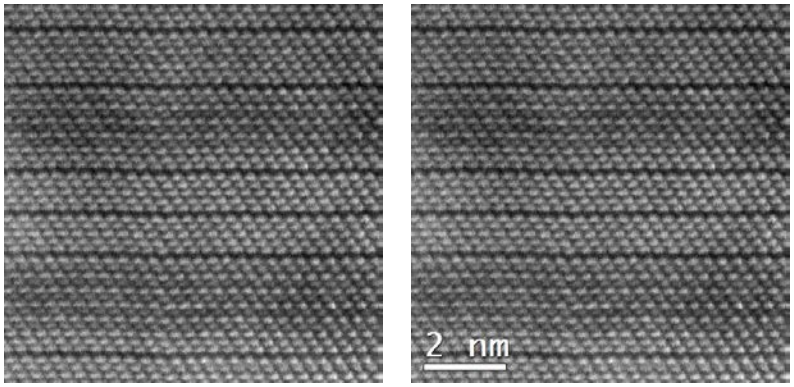

Figure S4: Image calibration was found using the Si(111) spacing.

4. **Application of GPA algorithm**: The GPA algorithm was applied on images of sufficient quality and resolution using the parameters in Table S1:

Table S1: GPA algorithm parameters

a* (1/nm)	5.0
b* (1/nm)	3.21167

gamma (°)	±58.1556
theta (°)	+90.0
resolution (nm)	1.0

Particularly the a* and theta parameters are important while b* and gamma are approximate, as the x-direction (parallel to the substrate-film interface) could show distortions due to scanning conditions mentioned in 1. This value of a* = 5 1/nm specifically maps inter-planar distances between 0.17 nm and 0.25 nm, which showed to discriminate sufficiently well between covalent Ge/Sb-Te and vdW Te-Te inter-planar distances. For visualization purposes the “temperature” color-map in GMS software with [-0.5, 0.5] low-high contrast limits was chosen (Figure S5).

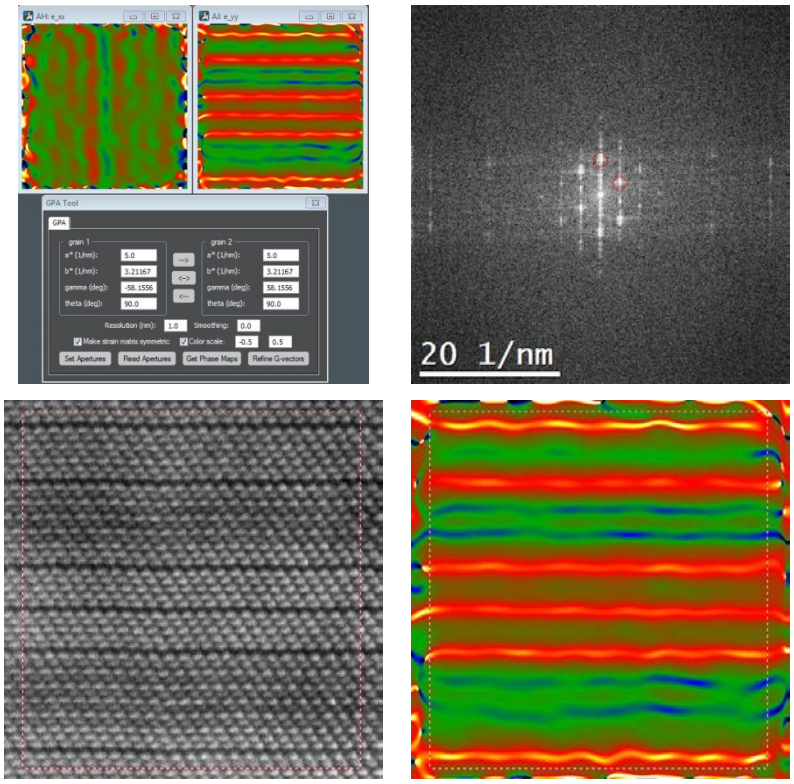

Figure S5: GPA analysis is performed using the parameters in Table S1.

5. **Analysis of e_yy phase maps**: The e_yy maps from the GPA algorithm were cropped to contain the relevant film region and processed using MATLAB software. A script was written to each time take a 1 nm wide vertical linescan and locate the position of vdW gaps using a peak-find algorithm throughout the micrograph. A histogram was made of the consecutive vdW gap distances using 1.015 nm + 0.356 nm * n (n = 0, 1, …, 7) equidistant bins (discarding the rest), representing the homologous

Sb_2Te_3 block and GeTe block distances,[3,4,7,17–19] respectively (Figure S6 and S7). The results of multiple image then comprised the final histogram shown in the main text, were the area-weighted averages and standard deviations are shown. The areas analyzed for SL1 (as dep., 300 °C annealed and 400 °C annealed) and SL2 (as deposited) are 6.8×10^3 nm^2, 12.5×10^3 nm^2 and 2.5×10^3 nm^2 and 4.2×10^3 nm^2, respectively.

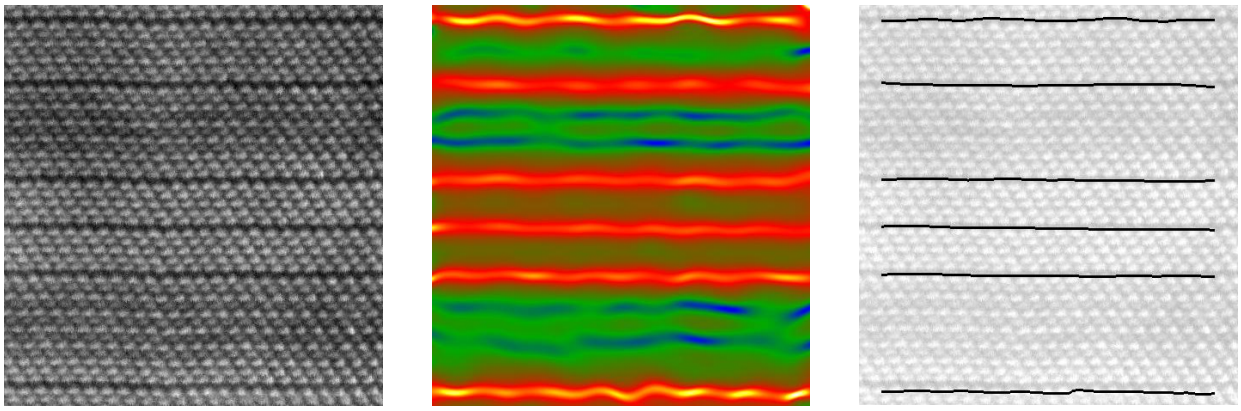

Figure S6: The GPA map is analyzed to find the positions of vdW gaps.

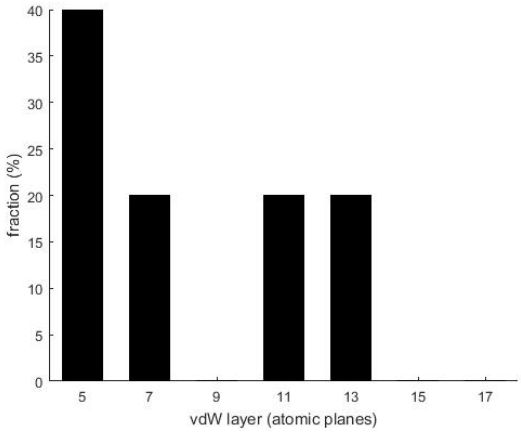

Figure S7: Histogram resulting from the previous analysis. In this case the result can be directly inspected and five vdW slabs are observed. QL are 2/5 slabs and 7-, 11- and 13-layers are 1/5 slabs, as is found by the procedure and shown in the histogram.

3. EDX calibration with Sb_2Te_3 and GeTe films

The average EDX analyses in this work are obtained in the TEM using both cross-sectional and plan-view specimen. To test both the precision and accuracy of the method, MBE grown Sb_2Te_3 and GeTe samples from related works are analyzed and the results are shown below.[20,21] As these binary samples are grown in the epitaxial regime, where the composition is shown to be constant and independent of deposition temperature,[22] these measurements can be used as a reference for the SL stoichiometry quantification. For the quantification process the Ge K, Sb L and Te L lines are used. For calibration of the energy scale the Cu K peak at ~8 keV is used as a reference, which is always present because the specimens contain a brass support.

Figure S8 and S9 show the spectra obtained for an Sb_2Te_3 and GeTe cross-section specimen using a ~50 nm spot, respectively, and Figure S10 shows the spectra for a GeTe plan-view specimen using a ~10 μm spot from the same GeTe sample. Their respective quantification results, using the Cliff-Lorimer method without absorption, are shown in Tables S2-S5. Inspecting both at the average fitting error and the standard deviation from different positions, it can be concluded that the analysis is to within 1 at.% precise for Ge, Sb and Te. In addition it can be concluded that the ~50 nm spot did not significantly alter the composition of the film and the knock-off damage is below instrumental precision.

To comment on the accuracy these results are compared with other literature studies. Previous chemical analyses using X-Ray Fluorescence (XRF) have shown that epitaxial Sb_2Te_3 indeed grows with 40:60 composition for Sb:Te and epitaxial GeTe is a bit off-stoichiometric with 46:54 for Ge:Te.[22] While some of the theoretical works in the field model GeTe to have a complete NaCl structure, with less than 1% Ge vacancies on the cation sublattice,[23,24] experimental works suggest that crystalline GeTe should be more sparse and contain 8% to 16% Ge vacancies on the cation sublattice.[25–27] This would suggest a crystalline GeTe stoichiometry between 46:54 and 48:52 for Ge:Te. For comparison the Ge vacancy concentration on the cation sublattice is calculated additionally in Table S5. Thus, it can be concluded that the accuracy of GeTe quantification is at ~1 at.% consistent with different experimental results (XRF, EXAFS, XRD and doping methods) and are therefore not corrected to match exactly 50:50.

EDX spectra for MBE grown Sb_2Te_3 and GeTe

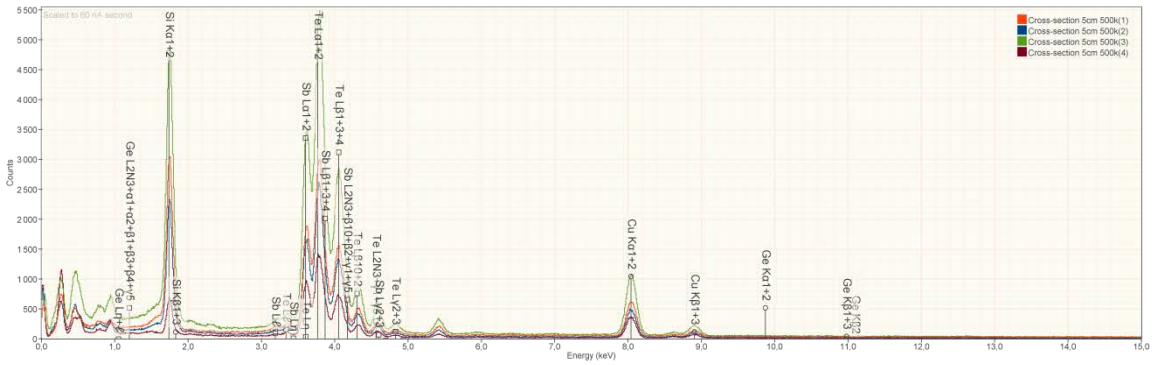

Figure S8: EDX spectra of a cross-sectional Sb_2Te_3 specimen using a ~50 nm spot.

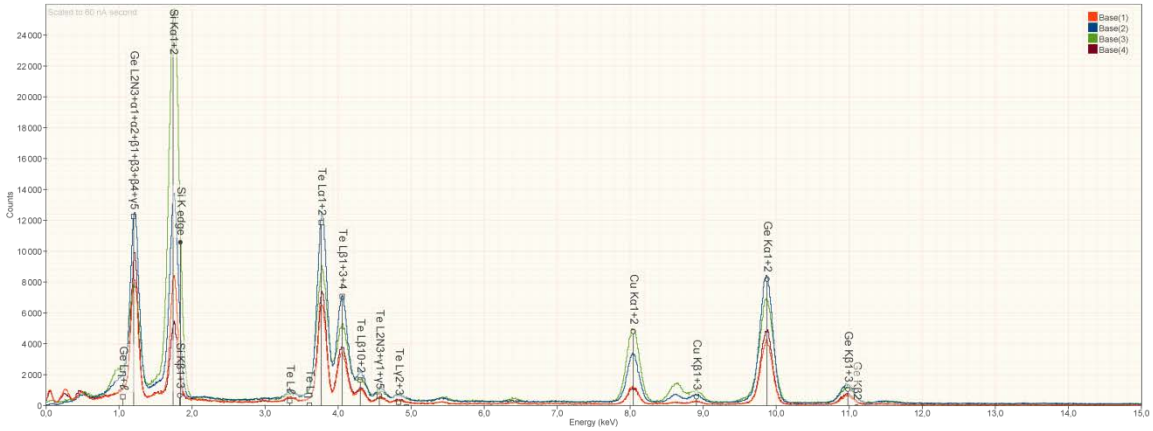

Figure S9: EDX spectra of a cross-sectional GeTe specimen using a ~50 nm spot.

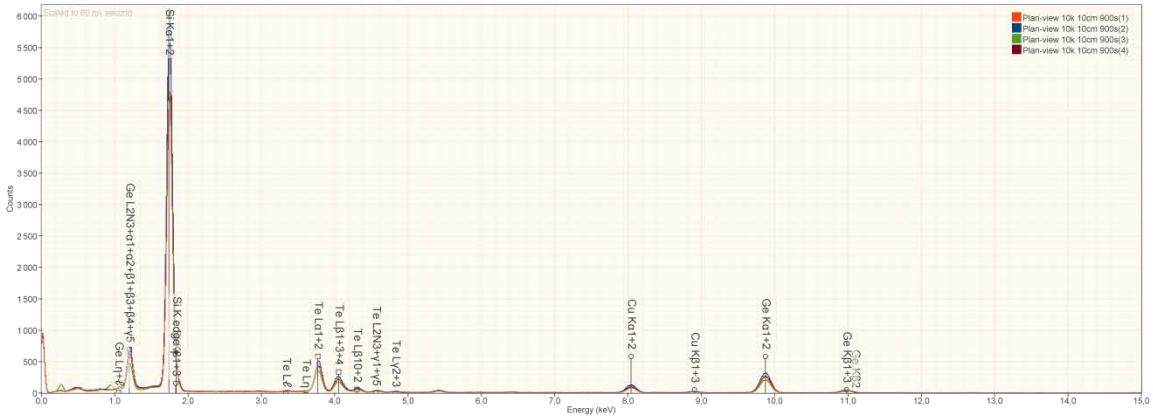

Figure S10: EDX spectra of a plan-view specimen from the same GeTe sample using a ~10 μm spot.

EDX quantification results for MBE grown Sb_2T_e3 and GeTe

Table S2: EDX quantification results for the spectra in Figure S8

	Sb L	err. (at.%)	Te L	err. (at.%)
	39.60	0.46	60.40	0.58
	40.05	0.48	59.95	-0.61
	40.71	0.34	59.29	0.44
	41.09	0.56	58.91	0.75
Average	40.36	0.46	59.64	0.29
St. dev.	0.67	0.09	0.67	0.61

Table S3: EDX quantification results for the spectra in Figure S9

	Ge K (at.%)	err. (at.%)	Te L	err. (at.%)
	46.61	0.51	53.39	0.53
	46.14	0.37	53.86	0.42
	47.23	0.49	52.76	0.55
	46.11	0.47	53.90	0.49
Average	46.52	0.46	53.48	0.50
St. dev.	0.52	0.06	0.53	0.06

Table S4: EDX quantification results for the spectra in Figure S10

	Ge K (at.%)	err. (at.%)	Te L	err. (at.%)
	46.34	0.37	53.66	0.38
	46.97	0.33	53.03	0.34
	46.40	0.41	53.60	0.41
	47.26	0.37	52.74	0.37
Average	46.74	0.37	53.26	0.38
St. dev.	0.45	0.03	0.45	0.03

Table S5: Summary of EDX quantification results

	Ge (at.%)	Sb (at.%)	Te (at.%)	Ge vac. (%)
Sb_2Te_3 cross-section		39.25±0.45	60.75±0.61	
GeTe cross-section	46.52±0.46		53.48±0.50	13.0±1.2
GeTe plan-view	46.74±0.37		53.26±0.38	12.2±1.0

4. EDX compositional analysis of SL films

Table S6: SL samples analyzed with EDX

Sample	SL1
Substrate	Si(111)-(√3x√3)R30°-Sb
Film deposition	$[Sb_2Te_3\text{-}GeTe]_{15}$ (3nm-1nm)
Cap deposition	Si_3N_4 (10nm)

Sample	SL2
Substrate	Si(111)-(√3x√3)R30°-Sb
Film deposition	$[Sb_2Te_3\text{-}GeTe]_9$ (3nm-1nm)
Cap deposition	Sb_2Te_3 (3nm)

Table S6 shows the applied growth characteristics of the analyzed SL films. The EDX measurements reported in our previous work[28] mentioned 15.11±0.36 at.% Ge, 27.88±0.74 at.% Sb and 57.01±0.99 at.% Te for SL1, where the error indicates the average Cliff-Lorimer (MBTS) fitting error. These results are summarized in Figure S11 and Table S7. It can be concluded that annealing did not significantly alter the composition. SL1 was re-analyzed using a ~50 nm spot on a cross-sectional specimen. The results of these measurements are shown in Figure S12 and Table S8.

Similarly, the SL2 was analyzed using a ~50 nm spot on a cross-section specimen and a ~10 μm spot on a plan-view specimen of which the results are shown in Figure S13 and Table S9 and Figure S14 and Table S10, respectively. It can be concluded that the ~50 nm spot did not significantly alter the composition of the film and the knock-off damage is below instrumental precision.

To summarize, the results of the EDX quantification of the SL samples are shown in Table S11, where the error indicated is the average fitting error of the different results. Table S12 shows the binary decomposition of GeTe and Sb_2Te_3 in the SL films, while Table S13 gives an estimate of vacancies on the cation sublattice with respect to a cubic structure and with respect to a complete ordering of vacancy layers as in the stable GST models,[3,4,7,19] respectively. The latter should be interpreted with reference to the epitaxial GeTe measurements, which shows ~47:53 ratio for Ge:Te or ~12% vacancies. This implies that if this number is more approaching 12% from below, more random vacancies have ordered to layers and vdW gaps. The results therefore indicate that SL2 has a higher degree of vacancy ordering compared with SL1.

EDX spectra for SL1

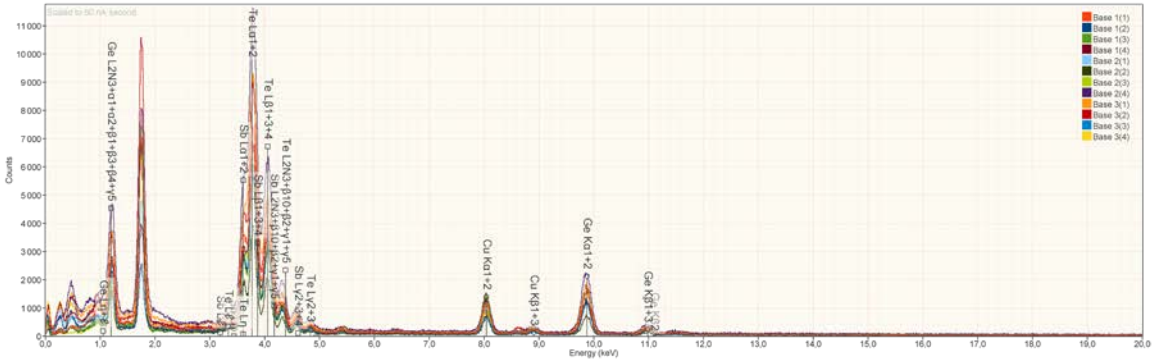

Figure S11:EDX spectra of the previously reported cross-sectional SL1 specimen using a ~50 nm spot.[28]

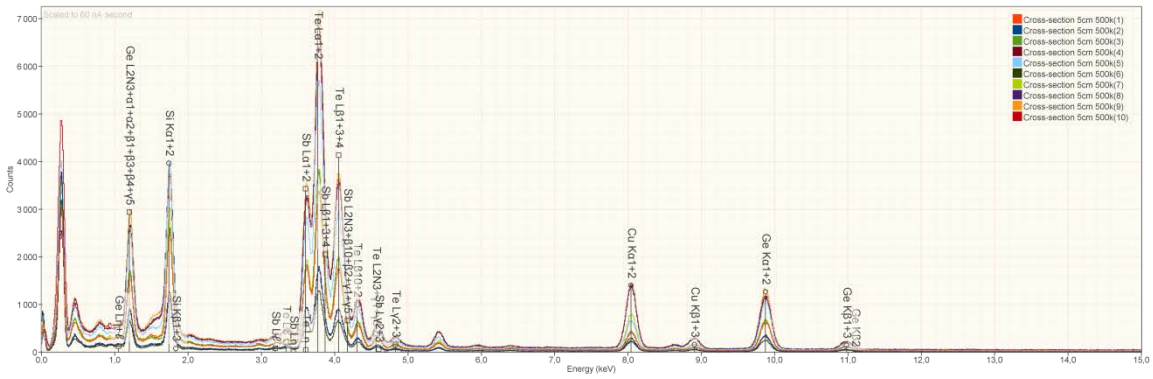

Figure S2: EDX spectra of the re-analyzed cross-sectional SL1 specimen using a ~50 nm spot.

EDX quantification results for SL1

Table S7: EDX quantification results for the spectra in Figure S11

	Ge K (at.%)	err. (at.%)	Sb L (at.%)	err. (at.%)	Te L (at.%)	err. (at.%)
as dep.	12.32	0.52	28.56	0.82	59.12	1.09
	13.15	0.44	29.01	1.01	57.83	1.38
	14.31	0.31	29.23	0.80	56.45	1.00
	14.97	0.43	29.12	0.74	55.92	0.93
ann. 250	15.84	0.35	27.94	0.69	56.22	0.94
	16.93	0.39	28.08	0.64	54.99	0.82
	20.02	0.29	26.52	0.61	53.47	0.79
	14.19	0.37	26.68	0.82	59.13	1.13
ann. 300	14.22	0.36	27.53	0.66	58.25	0.84
	14.44	0.46	28.39	0.81	57.17	1.03
	16.48	0.28	27.25	0.57	56.27	0.80
	14.99	0.29	27.11	0.81	57.90	1.13
ann. 400	14.97	0.32	28.00	0.83	57.03	1.14
	14.98	0.31	27.95	0.64	57.07	0.87
	15.21	0.38	28.13	0.66	56.66	0.84
	14.74	0.26	26.57	0.77	58.69	1.05
Average	15.11	0.36	27.88	0.74	57.01	0.99
St.dev.	1.72	0.07	0.88	0.11	1.51	0.16
Ave. as dep.	13.69	0.43	28.98	0.84	57.33	1.10
St.dev. as dep	1.18	0.09	0.29	0.12	1.44	0.20
Ave. ann. 250	16.75	0.35	27.31	0.69	55.95	0.92
St.dev. ann. 250	2.46	0.04	0.82	0.09	2.40	0.15
Ave. ann. 300	15.03	0.35	27.57	0.71	57.40	0.95
St.dev. ann. 300	1.02	0.08	0.57	0.12	0.88	0.16
Ave. ann. 400	14.98	0.32	27.66	0.73	57.36	0.98
St.dev. ann. 400	0.19	0.05	0.73	0.09	0.90	0.14

Table S8: EDX quantification results for the spectra in Figure S12

	Ge K (at.%)	err. (at.%)	Sb L	err. (at.%)	Te L	err. (at.%)
	14.95	0.20	29.54	0.37	55.50	0.48
	15.17	0.28	29.06	0.51	55.77	0.66
	14.31	0.19	28.17	0.35	57.52	0.47
	15.64	0.27	30.10	0.51	54.27	0.65
	15.03	0.15	28.10	0.29	56.87	0.38
	15.92	0.33	28.47	0.59	55.60	0.76
	14.18	0.19	28.14	0.35	57.67	0.46
	14.16	0.14	27.71	0.26	58.13	0.36
	14.73	0.14	28.29	0.26	56.99	0.35
	13.90	0.14	27.98	0.27	58.13	0.36

Average	14.80	0.20	28.56	0.38	56.65	0.49
St. dev.	0.67	0.07	0.76	0.12	1.30	0.15

EDX spectra for SL2

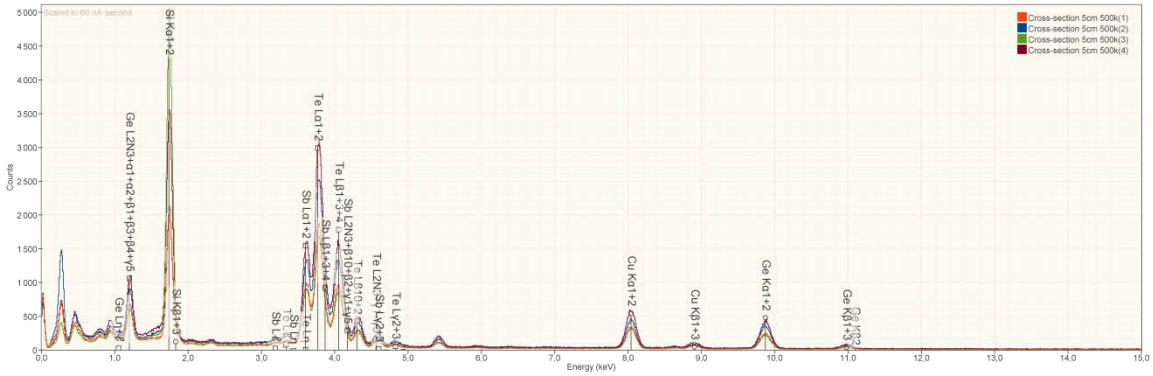

Figure S3: EDX spectra of the cross-sectional SL2 specimen using a ~50 nm spot.

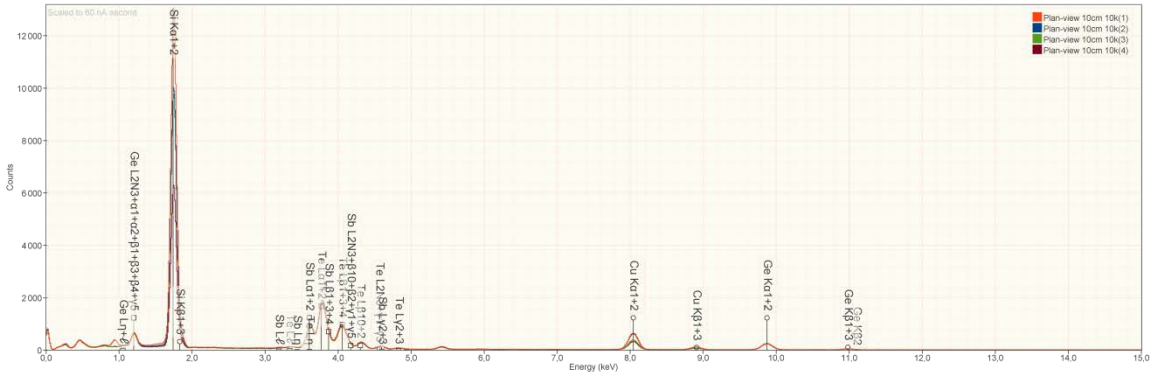

Figure S4: EDX spectra of the plan-view SL2 specimen using a ~10 μm spot.

EDX quantification results for SL2

Table S9: EDX quantification results for the spectra in Figure S13

	Ge K (at.%)	err. (at.%)	Sb L	err. (at.%)	Te L	err. (at.%)
	10.93	0.25	30.54	0.53	58.53	0.67
	11.31	0.21	30.46	0.45	58.23	0.58
	10.73	0.26	31.34	0.56	57.93	0.71
	11.29	0.20	30.38	0.41	58.33	0.53
Average	11.07	0.23	30.68	0.49	58.26	0.62
St. dev.	0.28	0.03	0.44	0.07	0.25	0.08

Table S10: EDX quantification results for the spectra in Figure S14

	Ge K (at.%)	err. (at.%)	Sb L	err. (at.%)	Te L	Err. (at.%)
	11.34	0.12	30.29	0.25	58.37	0.34
	11.23	0.12	30.53	0.25	58.24	0.33
	11.19	0.12	30.57	0.25	58.24	0.34
	11.41	0.12	30.33	0.25	58.26	0.34
Average	11.29	0.12	30.43	0.25	58.28	0.34
St. dev.	0.10	0.00	0.14	0.00	0.06	0.01

EDX quantification results summary for SL1 and SL2

Table S11: Summary of EDX quantification results

		Ge (at.%)	Sb (at.%)	Te (at.%)
SL1-1	SL1 cross-section (prev.[28])	15.11±0.36	27.88±0.74	57.01±0.99
SL1-2	SL1 cross-section	14.80±0.20	28.56±0.38	56.65±0.49
SL2-1	SL2 cross-section	11.07±0.23	30.68±0.49	58.26±0.62
SL2-2	SL2 plan-view	11.29±0.12	30.43±0.25	58.28±0.34

Table S12: Decomposition of the results in GeTe and Sb_2Te_3 fractions

SL1-1	Ge K (at.%)	err. (at.%)	Sb L	err. (at.%)	Te L	err. (at.%)	Total (at.%)	err. (at.%)
	15.11	0.36	27.88	0.74	57.01	0.99	100.00	
			27.88	0.74	41.82	1.11	69.70	1.34
	15.11	0.36			15.19	1.49	30.30	1.49

SL1-2	Ge K (at.%)	err. (at.%)	Sb L	err. (at.%)	Te L	err. (at.%)	Total (at.%)	err. (at.%)
	14.80	0.20	28.56	0.38	56.65	0.49	100.00	
			28.56	0.38	42.83	0.56	71.39	0.68
	14.80	0.20			13.81	0.75	28.61	0.75

SL2-1	Ge K (at.%)	err. (at.%)	Sb L	err. (at.%)	Te L	err. (at.%)	Total (at.%)	err. (at.%)
	11.07	0.23	30.68	0.49	58.26	0.62	100.00	
			30.68	0.49	46.02	0.73	76.70	0.88
	11.07	0.23			12.24	0.96	23.30	0.96

SL2-2	Ge K (at.%)	err. (at.%)	Sb L	err. (at.%)	Te L	err. (at.%)	Total (at.%)	err. (at.%)
	11.29	0.12	30.43	0.25	58.28	0.34	100.00	
			30.43	0.25	45.65	0.38	76.08	0.45
	11.29	0.12			12.63	0.50	23.93	0.50

Table S13: % vacancies based on cubic and stable GST models

	Metastable approximation				Stable approximation		
	Cation (%)	Vac. (%)	Err. (at.%)		Cation (%)	Vac. (%)	Err. (at.%)
SL1-1	75.4%	24.6%	1.3%		99.5%	0.5%	10.0%
SL1-2	76.5%	23.5%	0.7%		107.2%	-7.2%	6.0%
SL2-1	71.7%	28.3%	0.8%		90.4%	9.6%	7.3%
SL2-2	71.6%	28.4%	0.4%		89.4%	10.6%	3.7%

5. X-ray diffraction of as-grown and annealed SL films

Figure S15 and S16 show the extended XRD spectra shown in the main text. The peaks at Q_z = 2.00 Å^{-1}, 4.01 Å^{-1}, and 6.01 Å^{-1} correspond to Si(111), Si(222) and Si(333) reflections, respectively, while the peaks at Q_z = 1.8 Å^{-1}, 3.7 Å^{-1}, and 5.5 Å^{-1} correspond to the average out-of-plane Te spacing, or Te(111), Te(222) and Te(333) reflections. This latter spacing is not at a fixed value and is different for S1 and S2 and changes its value upon annealing. Figure S17 shows a plot of its d-spacing for different annealing temperatures.

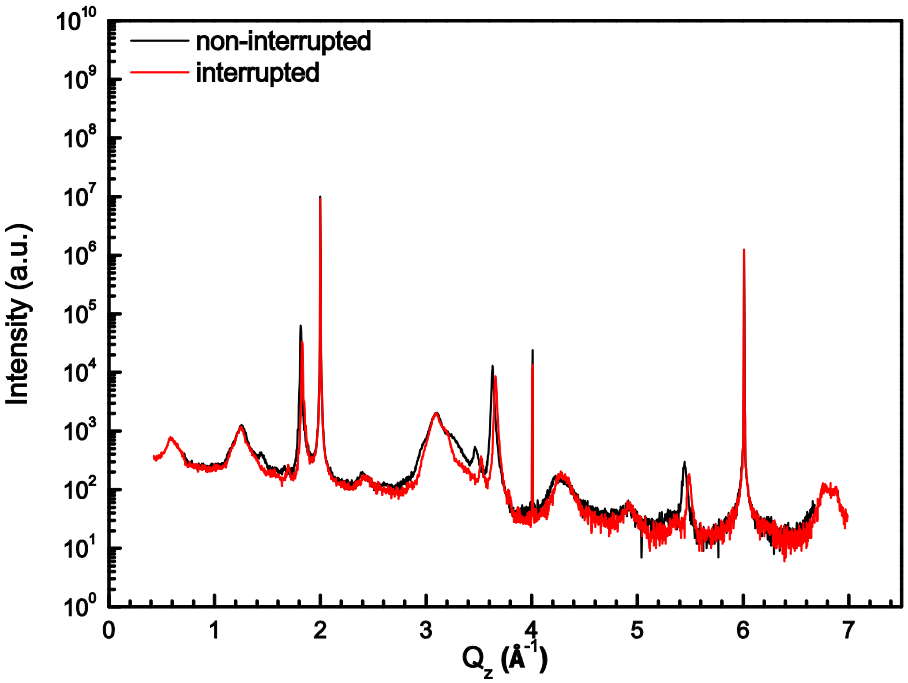

Figure S5: Extended XRD θ-2θ scan of SL1 and SL2.

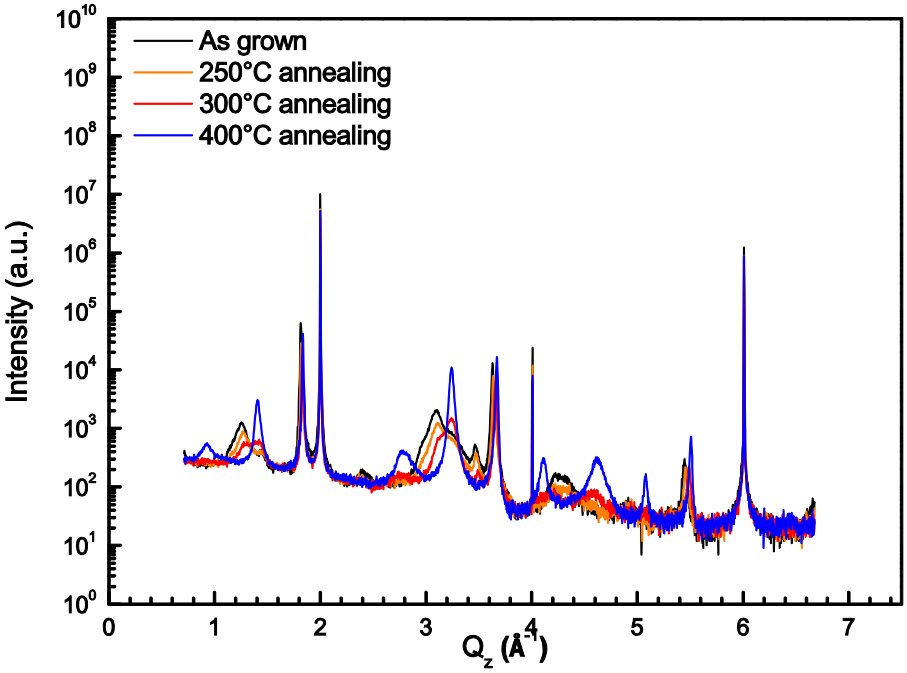

Figure S6: Extended XRD θ-2θ scan of SL1 after annealing.

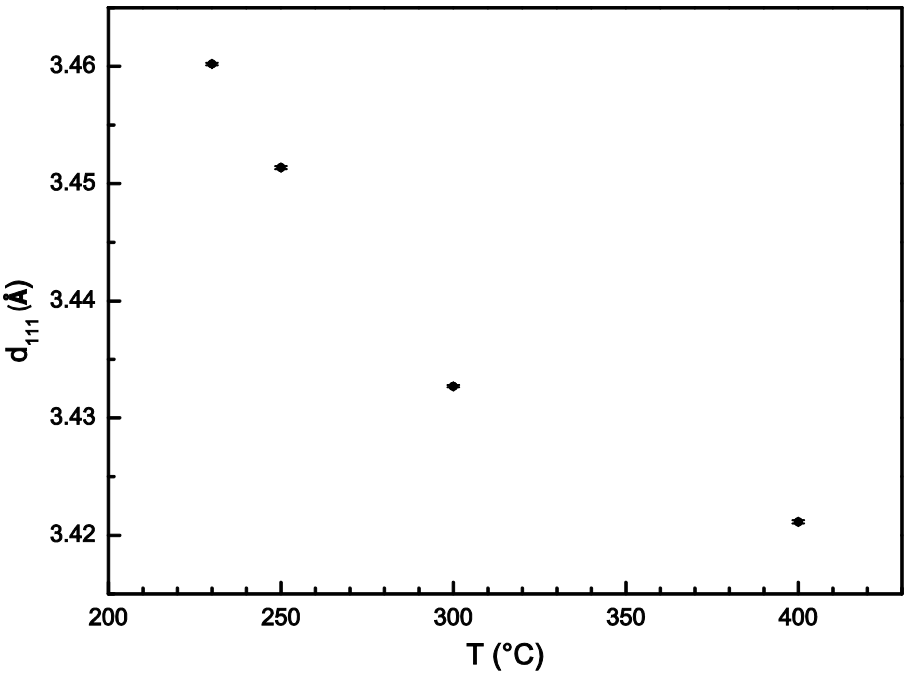

Figure 7: Evolution of the SL1 Te(111) peak after annealing.

6. Summary of EDX and XRD results for SL1 and SL2

Table S14 shows a summary of EDX and XRD results for SL1-1 (previous EDX measurements), SL1-2 (new EDX measurements), SL2-1 (cross-sectional EDX measurements) and SL2-2 (plan-view EDX measurements). Some remarks:

- SL1-1 and SL1-2, as well as SL2-1 and SL2-2 results are consistent with each other.
- The SL1 results show that annealing did not significantly alter the composition.
- The SL2 results show that radiation and knock-off damage is limited for the applied probe sizes.
- The XRD and TEM film thicknesses are fully consistent, indicating a high-quality flat film.
- XRR is not well suited to distinguish the mixing of the film. Therefore the EDX results should be more accurate than XRR results.

Table S14: Summary of EDX and XRD results

	SL1-1			SL1-2		
	XRD sat.	XRR	TEM-EDX	XRD sat.	XRR	TEM-EDX
Film thickness (nm)	56.6	56.4	57.0	58.1	56.4	57.0
Bilayer thickness (nm)	3.77	3.76	3.80	3.87	3.76	3.80
GeTe sublayer thickness (nm)		0.95	1.05		0.95	0.96
Sb2Te3 sublayer thickness (nm)		2.81	2.75		2.81	2.84
	SL2-1			SL2-2		
	XRD sat.	XRR	TEM-EDX	XRD sat.	XRR	TEM-EDX
Film thickness (nm)	45.9	47.0	48.0	45.9	47.0	48.0
Bilayer thickness (nm)	4.65	4.89	4.92	4.65	4.89	4.92
GeTe sublayer thickness (nm)		1.52	1.17		1.52	1.20
Sb2Te3 sublayer thickness (nm)		3.37	3.75		3.37	3.72

7. References

1. Karpinsky, O. G., Shelimova, L. E., Kretova, M. A. & Fleurial, J.-P. An X-ray study of the mixed-layered compounds of (GeTe)n (Sb2Te3)m homologous series. *J. Alloys Compd.* **268,** 112–117 (1998).
2. Yamada, N. & Matsunaga, T. Structure of laser-crystallized Ge2Sb2+xTe5 sputtered thin films for use in optical memory. *J. Appl. Phys.* **88,** 7020–7028 (2000).
3. Matsunaga, T. & Yamada, N. Structural investigation of GeSb2Te4 A high-speed phase-change material. *Phys. Rev. B* **69,** 104111 (2004).
4. Matsunaga, T., Yamada, N. & Kubota, Y. Structures of stable and metastable Ge2Sb2Te5, an intermetallic compound in GeTe–Sb2Te3 pseudobinary systems. *Acta Crystallogr. B* **60,** 685–691 (2004).
5. Matsunaga, T. *et al.* Structural investigation of Ge3Sb2Te6, an intermetallic compound in the GeTe–Sb2Te3 homologous series. *Appl. Phys. Lett.* **90,** 161919 (2007).
6. Urban, P. *et al.* Temperature dependent resonant X-ray diffraction of single-crystalline Ge2Sb2Te5. *CrystEngComm* **15,** 4823–4829 (2013).
7. Kooi, B. J. & Hosson, J. T. M. D. Electron diffraction and high-resolution transmission electron microscopy of the high temperature crystal structures of GexSb2Te3+x(x=1,2,3) phase change material. *J. Appl. Phys.* **92,** 3584–3590 (2002).
8. Rotunno, E., Lazzarini, L., Longo, M. & Grillo, V. Crystal structure assessment of Ge–Sb–Te phase change nanowires. *Nanoscale* **5,** 1557–1563 (2013).
9. Ross, U., Lotnyk, A., Thelander, E. & Rauschenbach, B. Microstructure evolution in pulsed laser deposited epitaxial Ge-Sb-Te chalcogenide thin films. *J. Alloys Compd.* **676,** 582–590 (2016).
10. Lotnyk, A., Ross, U., Bernütz, S., Thelander, E. & Rauschenbach, B. Local atomic arrangements and lattice distortions in layered Ge-Sb-Te crystal structures. *Sci. Rep.* **6,** 26724 (2016).

11. Mio, A. M. *et al.* Chemical and structural arrangement of the trigonal phase in GeSbTe thin films. *Nanotechnology* **28,** 065706 (2017).
12. Zhang, B. *et al.* Element-resolved atomic structure imaging of rocksalt Ge2Sb2Te5 phase-change material. *Appl. Phys. Lett.* **108,** 191902 (2016).
13. Hÿtch, M. J., Snoeck, E. & Kilaas, R. Quantitative measurement of displacement and strain fields from HREM micrographs. *Ultramicroscopy* **74,** 131–146 (1998).
14. Hÿtch, M. J., Putaux, J.-L. & Pénisson, J.-M. Measurement of the displacement field of dislocations to 0.03 Å by electron microscopy. *Nature* **423,** 270–273 (2003).
15. Schamp, C. T. High-Resolution Metrology in the TEM. *Microsc. Today* **20,** 46–49 (2012).
16. Basile, G. *et al.* Measurement of the silicon (220) lattice spacing. *Phys. Rev. Lett.* **72,** 3133–3136 (1994).
17. Shelimova, L. E. *et al.* Homologous series of layered tetradymite-like compounds in the Sb-Te and GeTe-Sb2Te3 systems. *Inorg. Mater.* **36,** 768–775 (2000).
18. Anderson, T. L. & Krause, H. B. Refinement of the Sb2Te3 and Sb2Te2Se structures and their relationship to nonstoichiometric Sb2Te3−ySey compounds. *Acta Crystallogr. B* **30,** 1307–1310 (1974).
19. Matsunaga, T. *et al.* Single Structure Widely Distributed in a GeTe−Sb2Te3 Pseudobinary System: A Rock Salt Structure is Retained by Intrinsically Containing an Enormous Number of Vacancies within its Crystal. *Inorg. Chem.* **45,** 2235–2241 (2006).
20. Boschker, J. E. *et al.* Surface Reconstruction-Induced Coincidence Lattice Formation Between Two-Dimensionally Bonded Materials and a Three-Dimensionally Bonded Substrate. *Nano Lett.* **14,** 3534–3538 (2014).
21. Wang, R. *et al.* Toward Truly Single Crystalline GeTe Films: The Relevance of the Substrate Surface. *J. Phys. Chem. C* **118,** 29724–29730 (2014).
22. Perumal, K. Epitaxial growth of Ge-Sb-Te based phase change materials. (Humboldt-Universität zu Berlin, Mathematisch-Naturwissenschaftliche Fakultät I, 2013).

23. Zhang, W. *et al.* Role of vacancies in metal–insulator transitions of crystalline phase-change materials. *Nat. Mater.* **11,** 952–956 (2012).
24. Zhang, W., Wuttig, M. & Mazzarello, R. Effects of stoichiometry on the transport properties of crystalline phase-change materials. *Sci. Rep.* **5,** 13496 (2015).
25. Kolobov, A. V., Tominaga, J., Fons, P. & Uruga, T. Local structure of crystallized GeTe films. *Appl. Phys. Lett.* **82,** 382–384 (2003).
26. Tong, F. *et al.* Effective method to identify the vacancies in crystalline GeTe. *Appl. Phys. Lett.* **97,** 261904 (2010).
27. Kalra, G. & Murugavel, S. The role of atomic vacancies on phonon confinement in α-GeTe. *AIP Adv.* **5,** 047127 (2015).
28. Momand, J. *et al.* Interface formation of two- and three-dimensionally bonded materials in the case of GeTe-Sb2Te3 superlattices. *Nanoscale* **7,** 19136–19143 (2015).